A Search-and-Track Algorithm for Controlling the Number of Guided Modes of Planar Optical Waveguides with Arbitrary Refractive Index Profiles

Tarek A. Ramadan

Department of Physics Kuwait University, Safat-13060, Kuwait
and
Electronics and Electrical Communication Engineering Department
Ain Shams University, Abbasia 11517, Cairo, Egypt
Tarek.ramadan@ku.edu.kw

Abstract ─ A search-and-track algorithm is proposed for controlling the number of guided modes of planar optical waveguides with arbitrary refractive index profiles. The algorithm starts with an initial guess point in the parameter space that supports a specific number of guided modes. Then, it searches for, and tracks, the boundaries of this space or another space supporting a different number of modes. It does so by monitoring the sign of a unified cutoff dispersion function. The algorithm is applied to both symmetric and asymmetric silicon-based parabolic-index waveguides. It shows that unlike asymmetric waveguides, the single-mode condition of symmetric waveguides is controlled by TM-, as opposed to TE-, polarization. This abnormal polarization control is strongest for high index contrast waveguides of sub-micrometer core sizes. The results are verified by the full-vectorial beam propagation method.

Index Terms ─ EM propagation, integrated optics, numerical analysis, optical waveguides, waveguide theory.

I. INTRODUCTION

Identifying the optical waveguide parameters which support a specific number of modes is a key step that precedes the design of any photonic integrated circuit. In a few special cases, exact analytical expressions of these parameters are available [1]. In most of the other cases, they are only identified by approximate or numerical computational approaches [2-11]. The inherent assumptions and/or approximations in many of these approaches limit their application to specific regions of the parameter space. Other numerically intensive computational approaches [11] consume a considerable amount of time in generating design curves which map waveguide parameters to the number of guided modes.

The purpose of this paper is to develop an algorithm for controlling the number of modes of planar waveguides of an arbitrary refractive index profile, which combines simplicity and generality. The algorithm applies to both strong- and weak-guiding conditions and discriminates between TE and TM polarizations. It starts with *a priori* knowledge of waveguide parameters which support an initial number of guided modes. Then, it monitors the sign of a unified cutoff dispersion function to allocate the boundaries of the parameter space which supports the required number of modes. It identifies this space without direct solution of the dispersion equation. The algorithm reveals an abnormal TM-polarization dependence of the single-mode condition (SMC) of symmetric parabolic-index waveguides. This dependence is verified by computations done by full-vectorial beam propagation method (FV-BPM) [12]. To the best of our knowledge, this peculiar result has not been previously reported. It mainly affects the design of high index contrast waveguides with sub-micrometer core sizes.

II. BACKGROUND THEORY

A. Differential mode counting

The number of guided modes supported by an optical waveguide may change by changing any of its geometrical or refractive index parameters. The requirement that the effective refractive index, n_e, of each guided mode must cross-over the substrate refractive index, n_s, as the mode becomes guided or leaks into the substrate, implies a change in the sign of the corresponding dispersion function at cutoff [3]. It allows computing the number of modes at any point of the parameter space in terms of the number of modes at another reference point by counting the number of changes in the sign of the cutoff dispersion function along an arbitrarily chosen path between these points. This count must exclude the changes in this sign due to poles of the dispersion function, which may crossover the cutoff point along that path. It is the basis of the search-and-track (SAT) algorithm presented in this paper.

B. Discretization model

Consider the case of a planar waveguide with core thickness *t,* upper cladding thickness *h*, and a semi-infinite substrate. Its cover and substrate refractive indexes are n_a and n_s, respectively. Its core refractive index has a maximum, n_c, and a minimum, which is greater than n_s. It is converted by discretization to a nonuniform stack of L step-index layers of thickness Δt_l and refractive index n_l. The recurrence dispersion function of this stack is obtained in terms of the normalized propagation constant, $b=(\delta_e-1)/(\delta_f-1)$, following the approach in [13]. Here, $\delta_e=n_e^2/n_s^2$, and $\delta_f=\max_l\left(n_l^2/n_s^2\right)$, which limits b between zero and unity. The cutoff dispersion function of this stack, C_L, is obtained by taking the limit of the dispersion function as $b\to 0$. It is given by (1) where, $\kappa_{l+1}=\eta_{l,l+1}\csc^2(\Delta T_l)$, $\rho_{l+1}=\cot(\Delta T_{l+1})+\eta_{l,l+1}\cot(\Delta T_l)$, $\eta_{l,l+1}=(\varepsilon_l/\varepsilon_{l+1})\sqrt{(\delta_{l+1}-1)/(\delta_l-1)}$, $\hat{\kappa}_2/\kappa_2=\left(1+\sigma^2\right)/\left((1+\gamma_a\sigma)+(\sigma-\gamma_a)\cot(\Delta T_1)\right)$, $\hat{\rho}_2=\rho_2+(\hat{\kappa}_2-\kappa_2)/C_1$, $\sigma=H/\varepsilon_1+1/\varepsilon_a\sqrt{a}$, and $\gamma_a=\left(1-a\varepsilon_a^2\right)/2\varepsilon_a\sqrt{a}$. The cutoff dispersion function, $C_1=\cot(\Delta T_1)-\sigma$. The normalized

$$C_L=\det\begin{pmatrix}\rho_L & \kappa_L & & & & & \\ 1 & \rho_{L-1} & \kappa_{L-1} & & & & \\ & 1 & \rho_{L-2} & \kappa_{L-2} & & & \\ & & \bullet & \bullet & \bullet & & \\ & & & 1 & \rho_{l+1} & \kappa_{l+1} & \\ & & & & \bullet & \bullet & \bullet \\ & & & & & 1 & \hat{\rho}_2 & \hat{\kappa}_2 \\ & & & & & & 1 & C_1\end{pmatrix}. \quad (1)$$

parameters, $\Delta T_l=(2\pi/\lambda_o)\Delta t_l\sqrt{n_l^2-n_s^2}$, and $H=(2\pi/\lambda_o)h\sqrt{n_1^2-n_s^2}$, where λ_o is the free-space wavelength. The asymmetry parameter, $a=\left(n_s^2-n_a^2\right)/\left(n_1^2-n_s^2\right)$, the stack-layer refractive index parameter, $\delta_l=n_l^2/n_s^2$, and the polarization parameters, $\varepsilon_l=\varepsilon_a=1$ for TE modes, while $\varepsilon_l=\delta_l$ and $\varepsilon_a=n_1^2/n_a^2$ for TM modes.

C. Interference of pole crossing with mode counting

The dispersion function has two groups of poles. The poles of the first group are given by, $b_l^{(1)}=(\delta_l-1)/(\delta_f-1)$. Each stack layer generates one of these poles. They never cross the cutoff point (b=0) due to changing any of the waveguide parameters. The poles of the second group are given by, $b_{l,p}^{(2)}=b_l^{(1)}\left(1-p^2\pi^2/\Delta T_l^2\right)$, where p = 1,2,.., $\lfloor\Delta T_l/\pi\rfloor$, for each stack layer of $\Delta T_l\ge\pi$. Here, $\lfloor x\rfloor$ denotes the floor of x. One of these poles crosses the cutoff point each time ΔT_l equals an integer multiple of π along any path in the parameter space. To investigate the effect of this crossing on the sign of C_L, the normalized thickness of the l^{th} layer in the vicinity of $q\pi$ is expressed as, $T_l=q\pi\pm\Delta$, where q is a positive integer and Δ is infinitesimally small. Only C_{l+1} (the minor indicated in (1)) depends on T_l through the $\cot(T_l)$ and $\sec^2(T_l)$ terms of the three parameters, ρ_l, ρ_{l+1}, and κ_{l+1}. These terms become infinitely high when Δ tends to zero. Therefore, with the assumption that no other normalized thickness is an integer multiple π, they dominate over other terms, which results in, $\rho_l=\pm 1/\Delta$, $\rho_{l+1}=\pm\eta_{l,l+1}/\Delta$, and $\kappa_{l+1}=\eta_{l,l+1}/\Delta^2$,

where we have used $\cos(\Delta)\approx 1$ and $\sin(\Delta)\approx \Delta$. These approximations become exact in the limit when $\Delta \to 0$. Now, $C_{l+1} = (\pm \eta_{l,l+1}/\Delta)C_l - (\eta_{l,l+1}/\Delta^2)C_{l-1}$ while $C_l = (\pm 1/\Delta)C_{l-1} - \kappa_l C_{l-2}$. Therefore, $C_{l+1} = (\mp \eta_{l,l+1}\kappa_l/\Delta)C_{l-2}$, which changes its sign when T_l crosses $q\pi$. Next, filtering out C_{l+1} from the determinant of (1), allows writing C_L as the product of C_{l+1} and the matrix,

$$U_L^l = \det\begin{pmatrix} \rho_L & \kappa_L & & & \\ 1 & \rho_{L-1} & \kappa_{L-1} & & \\ & 1 & \rho_{L-2} & \kappa_{L-2} & \\ & & \bullet & \bullet & \bullet \\ & & & 1 & \rho_{l+2} \end{pmatrix}, \quad (2)$$

where we have used $1/C_{l+1} = (\mp \Delta/\eta_{l,l+1}\kappa_l)(1/C_{l-2}) \to 0$ as $\Delta \to 0$. Since U_L^l is independent of T_l, then the limit, $\lim_{\Delta\to 0} C_L = (\lim_{\Delta\to 0} C_{l+1})(\lim_{\Delta\to 0} U_L^l) = \pm\infty$, which shows that C_L must change its sign when T_l crosses $q\pi$. This change in sign does not correspond to an increase or a decrease in the number of supported modes.

III. PROPOSED ALGORITHM

A. Search-and-track approach

In order to identify the closed space of generalized waveguide parameters *u* and *v*, which support a specific number of guided modes, *M*, the proposed algorithm starts with an initial guess of a point that either belongs to this space (see point 1 in Fig.1) or to a space supporting M_o modes, which is different from *M*. For example, a point in the n_c-*t* space with an initial maximum core refractive index, n_{co}, and an initial thickness, t_o. This initial guess may either be obtained using different physical and/or mathematical bounds (see below).

After choosing the initial guess point (IGP), the algorithm searches for a point on the space boundaries. For example, the boundary between the spaces supporting *M* and *M*+1 modes shown in Fig. 1. It does so by moving along a single dimension in the horizontal or the vertical direction of the *u*-*v* space in infinitesimally small steps starting from the IGP, keeping the other space dimension unchanged, see Fig. 1. In moving along either of the horizontal or vertical search paths, it monitors the sign of C_L. Any unwanted sign changes due to function poles crossing the cutoff point are filtered out, as described below. Once the number of sign changes exceeds the absolute difference between *M* and M_o, the motion along the horizontal (or vertical) dimension stops and the preceding point along the search path represents a point on the boundary that encloses the target space, which supports the required number of modes, *M*. See the flow chart in Fig. 2(a) for a description of the search loop.

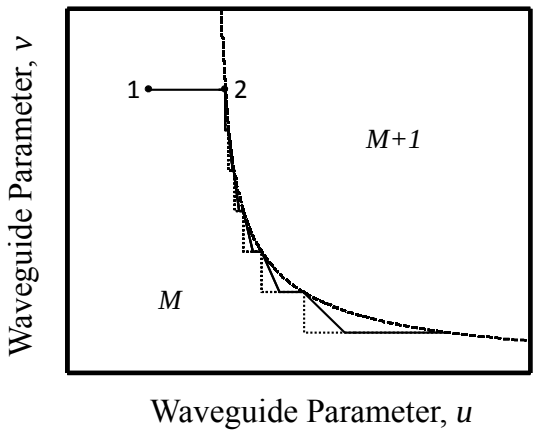

Fig. 1. A horizontal search path extending from an initial guess point 1 (with M_o = *M*) to point 2, which represents the origin of the track, followed by a downward staircase (dotted) or linear (solid) track of the boundary (dashed) between two *u*-*v* parameter spaces supporting *M* and *M*+1 modes. Although not shown, vertical search paths as well as upward staircase tracks may also be followed which results in four search and track possibilities.

The boundary point 2, allocated by the search loop, is the origin of a staircase path that tracks that boundary, see Fig. 1. It is created by a step decrease (or increase) in the vertical (or horizontal) parameter of the *u*-*v* space starting from this origin point, followed by a search for a new boundary point along the horizontal (or vertical) search dimension of the *u*-*v* space. This step-and-search process continues until sufficient points are allocated to reconstruct the space boundary within a predefined computational window. It requires *a priori* knowledge of the

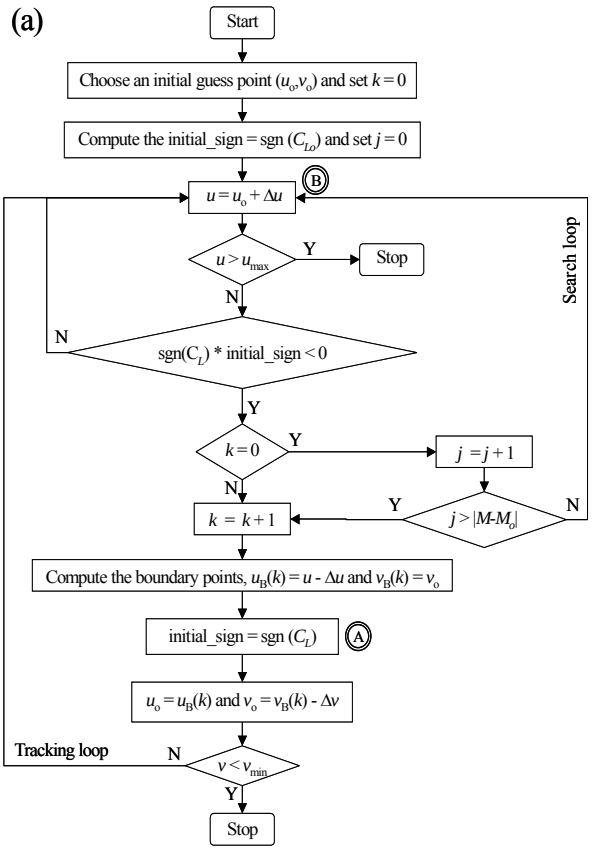

Fig. 2. (a) A flow chart description of a horizontal-search and downward-tracking algorithm. It assumes that u and v have opposite tracking directions. The index j counts the number of sign changes along the search path between points 1 and 2 of Fig.1. The index k counts the boundary points. The parameter L_o represents the number of discretization layers at the IGP, which, in general, may change to L as u or v changes. The vectors u_B and v_B are the u- and v-coordinates of the space boundary. Vertical search interchanges u and v in the search loop while upward tracking interchanges them in the tracking loop.

shape of the boundary to determine the directions of increasing or decreasing u and v along the track. These directions are governed by a general rule, which is described below. The staircase tracking loop is described in the flow chart of Fig. 2(a).

If the search path increases with the tracking steps, for example as in the n_c-t space,[1] then the

[1] The upper or lower boundary of an n_c-t space supporting M modes satisfies the asymptotic conditions, $n_c \to n_s$ when $t \to \infty$ and $n_c \to \infty$ when $t \to 0$. These conditions, in addition to the monotonic change of t and n_c along the boundary, imply that $\partial t / \partial n_c < 0$ and $\partial^2 t / \partial n_c^2 > 0$. Thus, the search path along n_c increases as t decreases along the track.

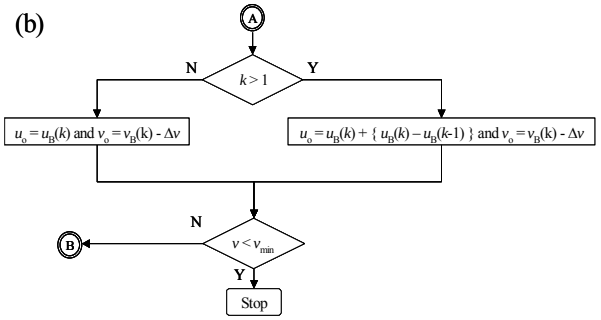

Fig. 2. (b) A flow chart description of linear downward tracking that substitutes the flow chart in (a) in going from A to B. Staircase tracking is initially followed (when k=1) until two or more boundary points (k>1) are allocated.

computations of the space boundary may be speeded up by using linear tracking. This tracking interpolates between the last two boundary points to predict the location of the third boundary point. Then, it searches for the actual boundary point starting from this predicted point, which is closer to the space boundary compared to the staircase tracking approach, see Fig. 1. It may be regarded as a modification of the staircase tracking in which a horizontal step is added to the vertical step in going from an actual boundary point to a predicted boundary point (a bottom corner point of the stair). The horizontal step equals the difference in u between the last two boundary points, as shown by the flow chart of Fig. 2(b). This interpolation process continues along the track, which shortens the overall search length and reduces the CPU computational time.

B. Tracking rule

As a preliminary step towards developing a tracking rule which specifies the directions of increasing or decreasing u and v along the boundary between two spaces, we classify waveguide parameters into two types depending on whether their increase may add modes to, or

subtract modes from, the waveguide. Next, the number of modes supported by the array is expressed as a two dimensional function $M(u,v)$ in the *u*-*v* space. The dependence of *M* on other waveguide parameters is suppressed for simplicity. Let $Y(u,v)$ be a randomly selected continuous differentiable function associated with *M*, which satisfies the relation, $\lfloor Y \rfloor = M$. The value of *Y* at the upper or lower boundary of the space supporting *M* modes is denoted by Y_B. In the vicinity of this boundary, $Y = Y_B + \Delta Y$, where ΔY represents a first-order perturbation from Y_B. This perturbation may be expanded by the first-order terms of a Taylor series, $\Delta Y = (\partial Y/\partial u)_B \Delta u + (\partial Y/\partial v)_B \Delta v$, around the boundary. For all functions *Y*, which satisfy $\lfloor Y \rfloor = M$, their derivatives in this expansion must be positive for mode-adding parameters and negative for mode-subtracting parameters. If this is not the case, then it would contradict the definition of these derivatives which are computed at the boundaries of the space where *u* and *v* have their extreme values (minima (maxima) for mode-subtracting parameters and maxima (minima) for mode-adding parameters at the upper (lower) boundary). The relation between Δu and Δv at the boundary (upper or lower) is obtained by setting $\Delta Y = 0$ in the Taylor expansion. It gives,

$$\Delta v = -(\partial Y/\partial u)_B / (\partial Y/\partial v)_B \, \Delta u \, . \qquad (3)$$

According to (3), Δu and Δv must have opposite (similar) signs whenever $(\partial Y/\partial u)_B$ and $(\partial Y/\partial v)_B$ have similar (opposite) signs. This result leads to a simple tracking rule, which states that: two waveguide parameters of the same type must have opposite tracking directions (if one decreases, then the other increases and vice versa) while those of different types must have the same tracking direction (both increase or decrease) along the boundaries of the parameter space supporting a specific number of modes. For example, the increase in either of the thickness *t* or the maximum core refractive index n_c of an optical waveguide never decreases the number of guided modes. It either increases it or keeps it constant. Therefore, *t* and n_c must have opposite tracking directions along the boundaries of a specific space. Inspection of the waveguide design parameters leads to the conclusion that, except for the substrate refractive index, n_s, all other parameters (including *t*, *h*, n_c, and n_a) are mode-adding parameters. Note that the cover refractive index is constrained by, $n_a \le n_s$. Since the free-space wavelength is a mode-subtracting parameter, normalization of any of the mode-adding parameters by λ_o does not change their type.

C. Filtering out sign changes due to poles

In order to filter out sign changes due to poles, it is sufficient to flip the sign of C_L at each crossing of a pole during the search loop; see the flow chart of Fig. 2(a). If these sign changes are not filtered out, they result in a premature termination of the search path and faulty locations of the boundary points of the parameter space. An alternative approach eliminates the crossing of poles by satisfying the condition, $\max_l \Delta t_l < \lambda_o \big/ 2\sqrt{n_c^2 - n_s^2}$, which ensures that all the layers of the stack are single moded ($\Delta T_l < \pi$). This elimination is only possible in graded-index waveguides. In other more general cases of refractive index profiles, which include step-index layers, e.g. in [14], the thickness of the step-index layers may exceed the maximum imposed by this condition. Hence, the above rule of flipping the sign of C_L at the crossing of each pole must be applied.

IV. APPLICATIONS

A. Modal maps

In this section, the SAT algorithm identifies waveguide parameters, which support different number of TE and TM modes. Since the number of modes supported by a step-index waveguide whose core refractive index is n_c (and shares all other waveguide parameters) represents an upper bound, the algorithm starts by choosing an IGP, which belongs to the space supporting the minimum number of modes (zero for asymmetric guides and one for symmetric guides). This choice allows selecting any combination of *u* and *v* of this step-index waveguide as an IGP. Next, the algorithm allocates the upper boundary of the space, which supports the initial number of modes, as explained in Section III. Then, the computations follow a sequential approach in allocating the

boundaries of the subsequent spaces. In these sequential computations, the upper boundary of one space is the lower boundary of the subsequent space. Thus, allowing sequential generation of the IGPs of the successive spaces, as their boundaries are constructed. The accuracy of the generated IGPs is verified by monitoring the flip in the sign of the cutoff dispersion function between successive spaces excluding those due to pole crossings. The final outcome is a two-dimensional modal map of selected waveguide parameters, which support different number of modes.

B. Asymmetric profiles

Consider the case of an optical waveguide made of a-SiO_x:H [15]. The waveguide parameters are h=0, n_a=1, n_s=1.45, $n(x)=1.6\sqrt{1-0.062\left((x/t_1)-1\right)^2}$ for $0<x<t_1$ and n(x) = 2.0 for $t_1<x<t_1+t_2\,(=t)$, where the x-axis has its origin at the cover-cladding interface and points towards the substrate. Its modal map was computed in the t_2-t_1 plane (replacing u with t_2 and v with t_1) using a MATLAB code which employs a vertical search with a downward staircase-tracking algorithm and follows the sequential approach described above. The algorithm starts with an IGP (t_1=0.1 μm, t_2=0.1 μm) in the space supporting zero modes. The computational steps along t_1 and t_2 are both equal to 10^{-2} μm. The choice of a uniform stack layer thickness of 10^{-3} μm in the graded-index layer eliminates the crossing of poles as t_1 increases. The pole filtering rule switches the sign of the cutoff dispersion function each time the normalized thickness of the step-index layer crosses $q\pi$ as t_2 increases. The resultant modal map is shown in Fig. 3. It identifies combinations of t_1 and t_2 which support different number of TE and TM modes.

As an example of the computations of the modal map in the η–t plane (replacing u with $\eta\left(\equiv\left(n_c^2-n_s^2\right)/2n_c^2\right)$ and v with t), consider a truncated parabolic-index waveguide with h=0, n_a=1, n_s = 1.45, and $n(x)=n_c\sqrt{1-2\eta(x/t)^2}$ for $0<x<t$. Its modal map was computed at λ_o=1.55 μm as described above, however, horizontal search was used, as opposed to vertical search, starting from an IGP (t=5 μm, n_c=1.45001). The results are shown in Fig. 4. It identifies

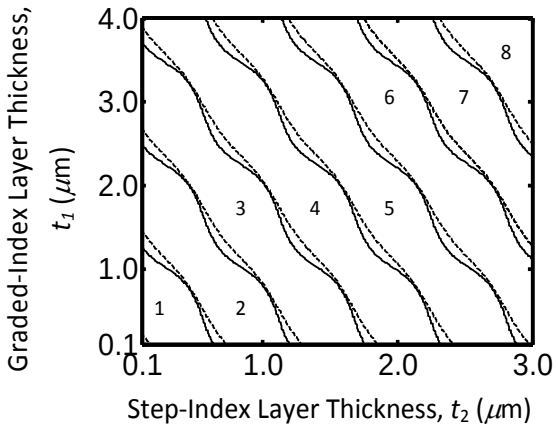

Fig. 3. Modal map of TE (solid) and TM (dashed) modes of a planar waveguide of a truncated parabolic index layer of thickness t_1 grown on top of a step-index layer of thickness t_2 computed at λ_o=1.55 μm. The other waveguide parameters are h=0, n_a=1, and n_s=1.45. The number of modes is indicated in each zone. Because of its small size, the zone supporting zero modes almost disappears.

combinations of t and η which support different number of TE and TM modes. The overall CPU times for these computations are 638 s and 659 s for the TE- and TM-modes, respectively. If linear tracking is used (see Section III-A) with the same IGPs to generate this modal map, then the CPU times reduce to 332 s and 380 s, for the TE- and TM-modes, respectively. This reduction represents 45% saving in the overall computational time.

The accuracy of the above modal maps has been verified using a FV-BPM simulator, which employs an iterative mode computational technique [12]. Because of the unlimited time needed to scan the parameter spaces of the entire modal maps, computations of the number of modes were carried out by changing the horizontal parameter of each map in steps at arbitrarily selected values of its vertical parameter (t_1 in the modal map of Fig. 3 and t in the modal map of Fig. 4). The results (not shown) show excellent agreement between these modal maps and the FV-BPM computations for both TE and TM polarizations.

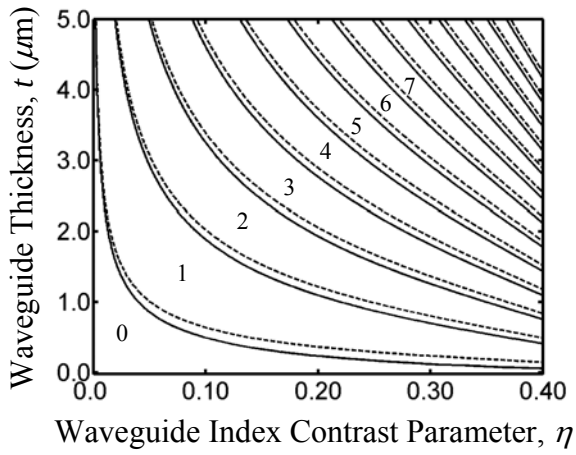

Fig. 4. Modal map of TE (solid) and TM (dashed) modes of a truncated parabolic-index waveguide with $h = 0$, n_a=1, and n_s=1.45 computed at λ_o=1.55 μm, showing parameters of the η–t space supporting zero to twelve modes.

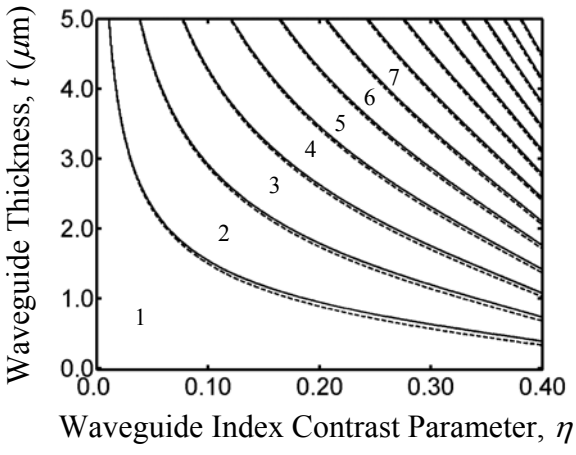

Fig. 5. Modal map of TE (solid) and TM (dashed) modes of a symmetric parabolic-index waveguide with n_s=1.45 computed at λ_o=1.55 μm, showing parameters of the η–t space supporting one to thirteen modes.

C. Symmetric profile

To investigate the effect of symmetry on the modal map, a symmetric parabolic-index waveguide is considered. Its core refractive index is $n(x) = n_c\sqrt{1-8\eta(x/t-1/2)^2}$ for $0 < x < t$ while n_s = 1.45. The SAT algorithm starts with the same IGP (t=5 μm, n_c=1.45001), which now belongs to the parameter space supporting a single mode. It uses the same numerical parameters and free-space wavelength as in the previous section. The computed modal map is plotted in Fig. 5. The CPU computational times of the TE and TM modes, using staircase tracking, are 666 s and 684 s, respectively. Again, linear tracking reduces these CPU times to 349 s and 360 s, respectively, which saves 47% of the overall computational time. The modal map of Fig. 6 shows that the splitting in cutoff boundaries between the TE and TM modes is inverted. Namely, unlike the asymmetric waveguides, the cutoff t (or η) of the TM modes is smaller than that of the TE modes at any η (or t). This inversion means that, under SMC, the maximum waveguide thickness equals the cutoff thickness of the first-order TM-, as opposed to TE- mode. Therefore, operating under single TE-mode condition does not ensure simultaneous single-mode operation of both modal polarizations in symmetric parabolic-index waveguides. This result has not been previously reported by various approximate methods which analyzed these symmetric waveguides, e.g. in [2, 5, 6].

D. FV-BPM computations

In order to verify this abnormal polarization dependence of the SMC, a symmetric parabolic-index waveguide parameters, $n_c = 2.55$ (η=0.34) and $t = 0.5$ μm, were selected, which support two TM modes and a single TE mode. They correspond to a point between the cutoff boundaries of the TM_1 and the TE_1 modes in the modal map of Fig. 5. Next, the FV-BPM simulator used in Section IV-B computed the modes of this guide at λ_o=1.55 μm. The results of these computations show that the waveguide supports two TM modes and a single TE mode. The computed modal field profiles are shown in Fig. 6. While these results are in agreement with the modal map computations, further verification was carried out to exclude any error in the mode excitation conditions of the FV-BPM computations. It is done by selecting a design point ($n_c = 2.55$ and $t = 0.6$ μm) from the modal map of Fig. 5, just above the cutoff boundary of the TE_1 mode. Then computing the effective index of the TM_1 mode (n_e=1.470229) and verifying that it is, indeed, greater than the effective index of the TE_1 mode (n_e=1.460989).

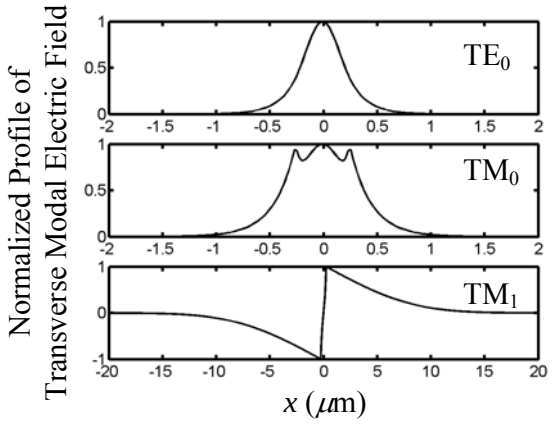

Fig. 6. Transverse electric-filed distribution of the TE_0 (top), TM_0 (middle), and TM_1 (bottom) modes of a symmetric parabolic-index waveguide with t=500 nm, n_c = 2.55, and n_s=1.45, computed by FV-BPM at λ_o=1.55 μm. The field is normalized to a maximum of unity.

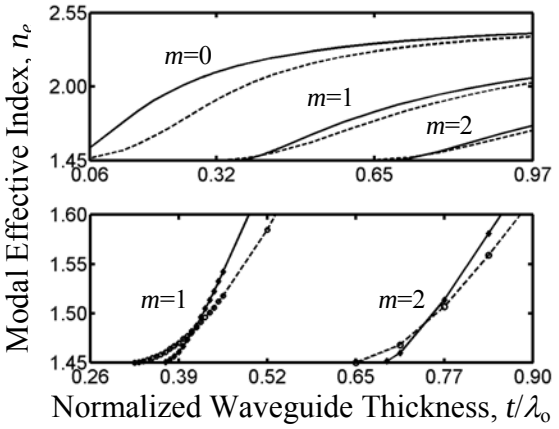

Fig. 7. Effective index n_e versus t/λ_o for the first three TE (solid) and TM (dashed) modes of a symmetric parabolic-index waveguide with n_c = 2.55 and n_s=1.45, computed by FV-BPM. Below is a zoom-in on the dispersion curves of the first-order (m=1) and the second-order (m=2) modes near their cutoff.

Full dispersion information was obtained by repetitive FV-BPM computations of n_e, as the waveguide thickness increased in steps from 0.1 μm to 1.5 μm, at λ_o=1.55 μm. The resultant dispersion curves are plotted in Fig. 7. It shows that, starting form the first-order mode (m=1), the dispersion curves of the TM and TE polarizations intersect near cutoff. This intersection leads to lower cutoff thickness of the higher-order TM modes compared to TE modes. Above the intersection thickness, the dispersion curves follow their normal behavior where the effective index of the TE modes is greater than the TM modes. Below this thickness, this relation is inverted and a range of thickness arises (between the cutoffs of the higher-order TM and TE modes) where an extra TM mode is supported. This range is where the modes of Fig. 6 were computed. This result is, again, consistent with the modal map computations and is a logical outcome of the inversion of the modal cutoff, which verifies the utility of the proposed algorithm.

E. Abnormal parameter space

In order to investigate the effect of the upper cladding layer thickness on the TM polarization dependence of the SMC, we consider an asymmetric parabolic waveguide with fixed n_s = 1.45, n_a = 1, η = 0.1 (n_c=1.62), and a variable h. It becomes a symmetric waveguide (as in Section IV-C) in the limit as $h \to \infty$. The cutoff thickness of the TE_1 and TM_1 modes of this guide were computed at different h at λ_o = 1.55 μm. The computations applied a vertical search with a downward stair-tracking algorithm to the h-t plane (replacing u with h and v with t). They started from an IGP (h=0.1 μm and t=0.1 μm) which supports zero modes (M_o=0), skipped a single sign change on the search path (corresponding to j=1 in the flow chart of Fig. 2(a)) to reach a point on the upper boundary of the target parameter space, which supports a single mode (M=1). Next, they followed opposite tracking directions along that boundary, according to the tracking rule of Section III-B. Figure 8 plots the computed cutoff waveguide thickness of the first-order TE and TM modes versus h. As expected, the cutoff thickness of the TM_1 mode starts higher (at low h), gradually decreases (with increasing h), and ends up lower than the cutoff thickness of the TE_1 mode. The upper cladding thickness h=730 nm at the point of intersection is the minimum h which results in an abnormal TM-polarization control of the SMC in this specific example. For further understanding of this abnormal polarization control, recomputations of the modal map of Fig. 4 (in the η–t space) were carried out replacing h=0 with h=730 nm. The new modal map (not shown) shows an intersection between the cutoff thickness of the TE_1 and TM_1

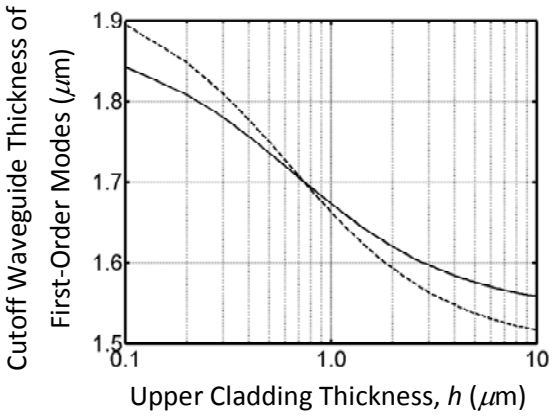

Fig. 8. Cutoff thickness of TE_1 (solid) and TM_1 (dashed) modes versus upper cladding thickness h for a parabolic-index waveguide with η=0.1, n_s=1.45, and n_a=1, computed at λ_o = 1.55 μm.

modes (upper boundaries of the M=1 space) at η=0.1 and t=1.7 μm. They show that at any t>1.7 μm (η<0.1) the SMC is controlled by the TE mode, otherwise (t<1.7 μm and η>0.1) it is controlled by the TM mode. Thus, the common waveguide cutoff thickness at the intersection point in Fig. 8 represents the maximum t which results in abnormal TM-polarization control of the SMC at h=730 nm.

In order to identify the boundary between the normal and abnormal spaces in the t-h plane, Fig. 9(a) plots h against this common cutoff thickness of the TE_1 and TM_1 modes, as η changes between 0.04 and 0.4. It identifies the combinations of t and h where the SMC is controlled by the TE (normal) or the TM (abnormal) mode. Figure 9(b) plots the same h against η to identify the same boundary between the normal and abnormal spaces in the η-h plane. Both figures show that the minimum h of the abnormal space decreases with decreasing t or increasing η. This decrease in the minimum h implies the need of a lower h in the case of high-index contrast waveguides of sub-micrometer core sizes to sustain the normal TE control of the SMC.

V. CONCLUSION

A numerical algorithm has been proposed for the design of planar optical waveguides with arbitrary refractive index profiles. The algorithm identifies the waveguide parameters, which support different number of modes. It is exact in the sense that the discretization error may

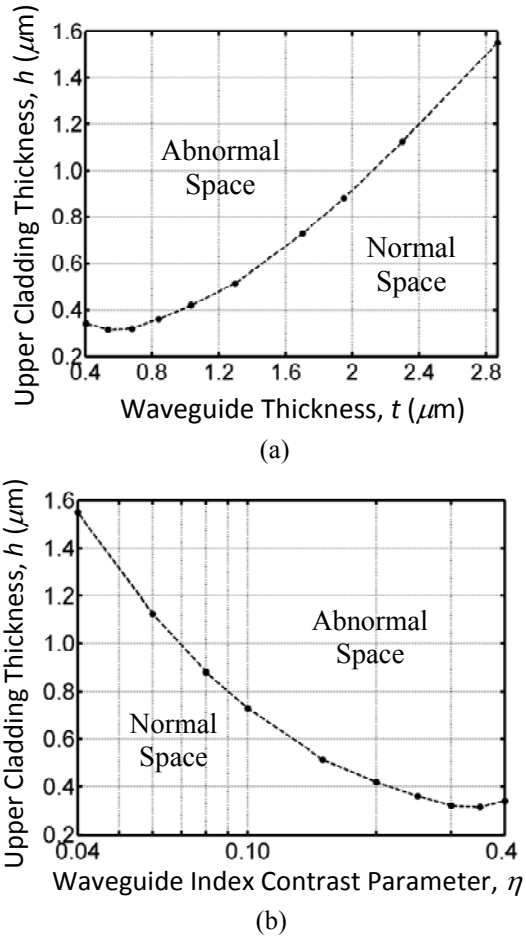

Fig. 9. Boundary between normal and abnormal regions of the (a) t-h and (b) η–h space of a parabolic-index waveguide with n_s=1.45 and n_a=1 computed at λ_o=1.55 μm.

arbitrarily be minimized by increasing the number of stack layers. It may be combined with genetic algorithms [16, 17] to optimize the performance of planar integrated optical devices under the constraint of supporting a specific number of modes using the appropriate cutoff function.

Application of the algorithm to symmetric and asymmetric parabolic-index waveguides reveals a fundamental difference between the modal polarizations which control the number of their guided modes. If the upper cladding thickness is greater than some critical thickness, which decreases under high index contrast and/or small core sizes, then this number is controlled by TM polarization. Otherwise, it is controlled by TE polarization.

REFERENCES

[1] M. J. Adams, *An Introduction to Optical Waveguides*, Wiley, New York, 1981.

[2] V. Ramaswamy and R. K. Lagu, "Numerical Field Solution for an Arbitrary Asymmetrical Graded-Index Planar Waveguide," *J. Lightw. Technol.*, vol. LT-1, no. 2, pp. 408-417, 1983.

[3] S. Ruschin, G. Griffel, A. Hardy, and N. Croitoru, "Unified Approach for Calculating the Number of Confined Modes in Multilayered Waveguiding Structures," *J. Opt. Soc. Amer. A*, vol. 3, no. 1, pp. 116-123, 1986.

[4] A. K. Ghatak, K. Thyagarajan, and M. R. Shenoy, "Numerical Analysis of Planar Optical Waveguides using Matrix Approach," *J. Lightw. Technol.*, vol. LT-5, no. 5, pp. 660-667, 1987.

[5] J. P. Donnelly and S. D. Lau, "Generalized Effective Index Series Solution Analysis of Waveguide Structures with Positionally Varying Refractive Index Profiles," *IEEE J. Quantum Electron.*, vol. 32, no. 6, pp. 1070-1079, 1996.

[6] H. Ding and K. T. Chan, "Solving Planar Dielectric Waveguide Equations by Counting the Number of Guided Modes," *IEEE Photon. Technol. Lett.*, vol. 9, no. 2, pp. 215-217, 1997.

[7] L. Wang and N. Huang, "A New Numerical Method for Solving Planar Waveguide Problems with Arbitrary Index Profiles: TE Mode Solutions," *IEEE J. Quantum Electron.*, vol. 35, no. 9, pp. 1351-1353, 1999.

[8] M. S. Chung and C. M. Kim, "General Eigenvalue Equations for Optical Planar Waveguides with Arbitrarily Graded-Index Profiles," *J. Lightw. Technol.*, vol. 18, no. 6, pp. 878–885, 2000.

[9] K. Mehrany and B. Rashidian, "Polynomial Expansion for Extraction of Electromagnetic Eigenmodes in Layered Structures," J. *Opt. Soc. Amer. B.*, vol. 20, no. 12, pp. 2434-2441, 2003.

[10] N. Zariean, P. Sarrafi, K. Mehrany, and B. Rashidian, "Differential-Transfer-Matrix Based on Airy's Functions in Analysis of Planar Optical Structures with Arbitrary Index Profiles," *IEEE J. Quantum Electron.*, vol. 44, no. 4, pp. 324-330, 2008.

[11] R. Scarmozzino, A. Gopinath, R. Pregla, and S. Helfert, "Numerical Techniques for Modeling Guided-Wave Photonic Devices," IEEE *J. Sel. Topics Quantum Electron.*, vol. 6, no. 1, pp. 150-162, 2000.

[12] G. R. Hadley and R. E. Smith, "Full-Vector Waveguide Modeling using an Iterative Finite-Difference Method with Transparent Boundary Conditions," *J. Lightw. Technol.*, vol. 13, no. 3, pp. 465-469, 1995.

[13] T. A. Ramadan, "A Recurrence Technique for Computing the Effective Indexes of the Guided Modes of Coupled Single-Mode Waveguides," *Progress In Electromagnetics Research M*, vol. 4, pp. 33-46, 2008.

[14] A. Delage, S. Janz, B. Lamontagne, A. Bogdanov, D. Dalacu, D. X. Xu, and K. P. Yap, "Monolithically Integrated Asymmetric Graded and Step-Index Couplers for Microphotonic Waveguides," *Opt. Express*, vol. 14, no. 1, pp. 148-161, 2006.

[15] K. Shiraishi and C. S. Tsai, "A Micro Light-Beam Spot-Size Converter using a Hemicylindrical GRIN-Slab Tip with High-Index Contrast," *J. Lightw. Technol.*, vol. 23, no. 11, pp. 3821-3826, 2005.

[16] D. S. Weile and E. Michielssen, "Genetic Algorithm Optimization Applied to Electromagnetics: A Review," *IEEE trans. Antennas Propagat.*, vol. 45, no. 3, pp. 343-353, 1997.

[17] D. Erni, D. Wiesmann, M. Spuhler, S. Hunziker, and E. Moreno, "Application of Evolutionary Optimization Algorithms in Computational Optics," *Applied Computational Electromagnetic Society (ACES) Journal*, vol. 15, no. 2, pp. 43-60, 2000.

Tarek A. Ramadan was born in Eldakahlia, Egypt, in 1966. He received the B.S. and M.S. degrees from the Electronics and Electrical Communication Engineering Department, Ain Shams University, Cairo, Egypt, in 1989 and 1994, and the Ph.D. degree from the Electrical Engineering Department, Columbia University, New York, in 2000.

From 1989 to 1990, he spent his military service at the Military Technical College, Cairo.

From 1990 to 1995, he was a Demonstrator and Assistant Lecturer at the Electronics and Electrical Engineering Department, Ain Shams University. From 2000 to 2007, he was an Assistant Professor at the Electronics and Electrical Communication Engineering Department, Ain Shams University. Since 2007, he has been an Associate Professor in the same department. In September 2004, he joined the Physics Department, Kuwait University, Kuwait. His research interests include analytical and numerical analysis of integrated optical components.

Dr. Ramadan was included in the 22nd edition of *Marquis Who's Who in the World* in 2005. He is a Member of IEEE Photonics society and the Optical Society of America.